

# Renormalization Group Study of the Electron-phonon Interaction in High $T_c$ Cuprates

Henry C. Fu<sup>a</sup>, Carsten Honerkamp<sup>b,c</sup>, and Dung-Hai Lee<sup>a,d,e</sup>

(a) Department of Physics, University of California at Berkeley, Berkeley, CA 94720, USA

(b) Institute for Theoretical Physics, Universität Würzburg, D-97074 Würzburg, Germany

(c) Max-Planck-Institute for Solid State Research, D-70569 Stuttgart, Germany

(d) Material Science Division, Lawrence Berkeley National Laboratory, Berkeley, CA 94720, USA. and

(e) Center for Advanced Study, Tsinghua University, Beijing 100084, China.

(Dated: May 24, 2019)

We generalize the numerical renormalization group scheme of Ref. [1–3] to study the phonon-mediated retarded interactions in the high  $T_c$  cuprates. We find that three sets of phonon-mediated retarded quasiparticle scatterings grow under RG flow. These scatterings share the following common features: 1) the initial and final quasiparticle momenta are in the antinodal regions, and 2) the scattering amplitudes have a  $x^2 - y^2$  symmetry. All three sets of retarded interaction are driven to strong coupling by the magnetic fluctuations around  $(\pi, \pi)$ . After growing strong, these retarded interaction will trigger density wave orders with d-wave symmetry. However, due to the d-wave form factor they will leave the nodal quasiparticle unaffected. We conclude that the main effect of electron-phonon coupling in the cuprates is to promote these density wave orders.

One of the most prominent puzzles to emerge from experimental studies of the high-temperature superconducting cuprate materials is the strong momentum-space dependence of the properties of the electronic excitations. This can be seen most clearly in angle-resolved photoemission spectroscopy (ARPES) of LSCO: at optimum doping, sharp quasiparticle peaks can be distinguished near the Fermi surface in both nodal and antinodal directions. However, when the system is underdoped, the antinodal quasiparticle peaks disappear, while the nodal quasiparticle peaks remain[4]. Another beautiful demonstration of the robustness of the nodal quasiparticle is obtained in the NaCCOC materials. Recent STM studies have shown the presence of a commensurate, 4 lattice constant, checkerboard order which is independent of doping[5] (indicating the importance of lattice pinning). Despite this, ARPES studies of the same system reveal nodal quasiparticle peaks[6]. Finally, ARPES experiments probing the isotope effect in optimally doped Bi2212 reveal a substantial isotope shift in the ARPES spectra near the antinode, but little shift in the nodal spectrum[7]. The broad picture emerging from these experiments is of nodal quasiparticles which are insensitive to doping, disorder, charge and spin order, and lattice vibration, while antinodal excitations are sensitive to all these perturbations. One of us (DHL) has dubbed this the “nodal-antinodal dichotomy”[4].

In the cuprates it is widely accepted that in the overdoped regime, quasiparticles are well-defined excitations all along the normal state Fermi surface. We view the effect of decreasing doping as changing the Fermi surface geometry and increasing the strength of the residual quasiparticle interaction. We model this residual interaction with a momentum independent quasiparticle scattering. It is important not to confuse this effective residual quasiparticle scattering with the bare local electron correlation. Previously Honerkamp *et al* have performed a

one-loop renormalization group (RG) study of this residual interaction[1]. Here we generalize their method to study the phonon-mediated retarded interaction. The RG treatment of the retarded interaction is similar to that used for one dimensional systems in Ref.[8–10]. Our motivation for studying the electron-phonon interaction in the cuprates are twofold: 1) we hope to better understand the electron-phonon interaction in doped Mott insulators, and 2) we hope to gain some insight about the origin of the nodal-antinodal dichotomy.

In a recent paper Devereaux *et al* pointed out the importance of the momentum dependence in the electron-phonon coupling constant when interpreting ARPES data[11]. In particular they showed that as the initial electron momentum is varied along the Fermi surface, the matrix element that couples the electron to the  $B_{1g}$  phonon exhibits a  $x^2 - y^2$  symmetry. Meanwhile studies including weak to intermediate Hubbard interaction have come to the conclusion that the s-symmetry electron-phonon coupling is suppressed by electron-electron repulsion[12–15], especially for large momentum transfer processes[13–15].

In this study we follow the RG flow of both the instantaneous and retarded electron-electron scattering amplitude in the full first Brillouin zone. We compare the flow of retarded interaction with different symmetry. We start with a tight binding dispersion given by  $\epsilon(\mathbf{k}) = -2t[\cos(k_x) + \cos(k_y)] + 4t' \cos(k_x) \cos(k_y) + 4t''[\cos^2(k_x) + \cos^2(k_y) - 1]$ , with  $t' = 0.3t$ ,  $t'' = -0.1t$ , and  $\mu = -0.7t$ . This set of parameter choice produces a rather realistic Fermi surface. Following Ref.[1] we choose the bare residual quasiparticle scattering amplitude  $U = 3t$ . As in Ref.[1] we perform a one-loop Wilsonian RG for the one-particle-irreducible four-point vertex functions. At each energy scale the renormalized four-point function serves as an effective interaction for particles with excitation energies  $|\epsilon(\mathbf{k})|$  below the cutoff scale  $\Lambda$ . The results we

report are obtained for a temperature  $k_B T = 0.04t$ , and the RG flow is integrated between initial cutoff  $\Lambda = 4t$  and final cutoff  $0.2t$ . With spin-rotational invariance, the cutoff-dependent effective interaction is given by

$$S_{int} = \sum_{\sigma, \sigma'} \int \prod_{i=1}^3 d^3 \mathbf{k}_i d^3 \omega_i V_{\Lambda}(\mathbf{k}_1, \mathbf{k}_2, \mathbf{k}_3) \psi_{\sigma}^{\dagger}(\mathbf{k}_4, \omega_4) \psi_{\sigma'}^{\dagger}(\mathbf{k}_3, \omega_3) \psi_{\sigma'}(\mathbf{k}_1, \omega_1) \psi_{\sigma}(\mathbf{k}_2, \omega_2). \quad (1)$$

In the above  $\psi_{\sigma}(\omega_i, \mathbf{k}_i)$  annihilates an electron with quantum numbers  $\omega_i, \mathbf{k}_i, \sigma$ ; furthermore  $\omega_4 = \omega_1 + \omega_2 - \omega_3$  and  $\mathbf{k}_4 = \mathbf{k}_1 + \mathbf{k}_2 - \mathbf{k}_3$ . The contribution to the RG flow  $\partial_{\Lambda} V_{\Lambda}$  is summarized by the Feynman diagrams in Fig. (1), where the label “I” or “R” denotes instantaneous or retarded interaction respectively. For the moment we discuss the instantaneous interaction, hence all interactions are the “I” type. In each diagram, there are two internal lines. One represents the Greens function

$$G_{\Lambda}(\mathbf{k}, \omega) = \frac{\chi_{\Lambda}(\mathbf{k})}{i\omega - \epsilon(\mathbf{k}) - \chi_{\Lambda}(\mathbf{k})\Sigma(\mathbf{k}, i\omega)}, \quad (2)$$

while the other represents

$$S_{\Lambda}(\mathbf{k}, \omega) = \frac{\chi'_{\Lambda}(\mathbf{k})[i\omega - \epsilon(\mathbf{k})]}{[i\omega - \epsilon(\mathbf{k}) - \chi_{\Lambda}(\mathbf{k})\Sigma(\mathbf{k}, i\omega)]^2}. \quad (3)$$

Here  $\chi_{\Lambda}(\mathbf{k}) = 1 - 1/\{\exp[|\epsilon(\mathbf{k})| - \Lambda]/0.05\Lambda\} + 1\}$  cuts off the contributions from  $|\epsilon(\mathbf{k})| < \Lambda$ , and  $\chi'_{\Lambda}(\mathbf{k}) \equiv \partial_{|\Lambda|}\chi$  is nonzero only for  $|\epsilon(\mathbf{k})|$  near the cutoff  $\Lambda$ . Each diagram stands for two contributions since there are two ways to associate the two internal lines with  $G_{\Lambda}$  and  $S_{\Lambda}$ . As in previous works[1–3] our calculation ignores higher order vertices and self-energy corrections (i.e  $\Sigma_{\Lambda}$  is set to zero). Therefore the RG flow has to be stopped before the interactions get too large and the lowest energy scales cannot be accessed in a controlled way.

We perform the RG numerically by dividing the Brillouin zone into 32 patches. Each patch is centered on a “radial” line, as shown in Fig. (1). By standard Taylor expansion and power counting arguments, the most relevant vertex functions are the ones with incoming and outgoing  $\mathbf{k}_i$  on the fermi surface and the  $\omega_i = 0$ . In the following we only keep track of these most relevant vertex functions, which means we ignore the momentum dependence in directions transverse to the Fermi surface. For the instantaneous electron-electron scattering we thus approximate the value of  $V_{\Lambda}(\mathbf{k}_1, \mathbf{k}_2, \mathbf{k}_3)$  by its value  $V_{\Lambda}(\mathbf{k}_F(i), \mathbf{k}_F(j), \mathbf{k}_F(l))$ , where  $\mathbf{k}_F(j)$  is the momentum on the fermi surface at the center of the  $j$ th patch. This leaves us with  $32^3$  couplings  $V(\mathbf{k}_F(i), \mathbf{k}_F(j), \mathbf{k}_F(l))$  to keep track of. We calculate the contributions to the flow of these couplings using the diagrams in Fig. (1). The frequency sums are performed analytically, and the loop momentum integration is performed by a sum over patches and integration along the radial lines.

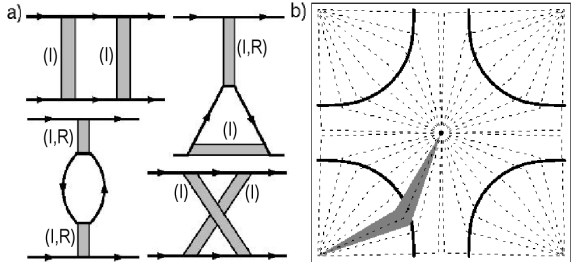


FIG. 1: a) One loop Feynman diagrams contributing to  $\partial_{\Lambda} V_{\Lambda}$ . Spin is conserved along solid lines. The labels “I” and “R” represent the instantaneous and retarded interaction (the gray bars) respectively. While all interactions can be the “I” type, only those with both “I” and “R” labels can be retarded. A diagram contributes to the flow of the instantaneous interaction when all interactions are the “I” type. A diagram contributes to the flow of retarded interaction when at least one vertex is the “R” type. b) The 32-patch discretization of the Fermi surface. Each patch (example in gray) is centered around one of the dashed lines.

The retarded interactions have non-trivial frequency dependence. We assume them to have the form

$$V_R(\mathbf{k}_1, \omega_1; \mathbf{k}_2, \omega_2; \mathbf{k}_3, \omega_3) = -\frac{g(\mathbf{k}_1, \mathbf{k}_3)g(\mathbf{k}_2, \mathbf{k}_4)\Omega_D}{(\omega_1 - \omega_3)^2 + \Omega_D^2}. \quad (4)$$

Here  $g(\mathbf{k}_1, \mathbf{k}_3)$  is the electron-phonon matrix element for scattering an electron from momentum  $\mathbf{k}_1$  to  $\mathbf{k}_3$ , and  $\Omega_D$  is a characteristic phonon (Debye) frequency. The retarded interaction dies off for frequency transfer  $|\omega_1 - \omega_3| > \Omega_D$ . In this work we approximate this dependence by a step-function cutoff[8]. This retarded interaction is represented by a new set of  $32^3$  “retarded” couplings,  $V_R(\mathbf{k}_F(i), \mathbf{k}_F(j), \mathbf{k}_F(l))$ . Because the internal lines in each of the diagrams have frequency poles at or greater than the cutoff energy  $\Lambda$  while those of the external legs are at zero energy, in the limit  $\Lambda \gg \Omega_D$  the leading contributions to the RG flow of the retarded interaction comes from diagrams in Fig. (1) where at least one interaction line is the “R” type. The contributions from diagrams with retarded interactions placed at vertices without an “R” label in Fig. (1) are down by a factor  $\Omega_D/\Lambda$ . Because the phonon energies of interest in the cuprates are  $\sim 60$  meV[16], in this work we integrate the RG flow equations to a lower cutoff of  $0.2t$ . Since the retarded interaction is present only when the frequency transfer is smaller than  $\Omega_D$ , diagrams with retarded interactions contribute only to the flow of retarded vertex function. Consequently the flow of instantaneous couplings is unaffected by the addition of retarded couplings, but the flow of retarded couplings is affected by the instantaneous interactions.

The RG flow of the instantaneous quasiparticle scattering alone with band parameter  $t'' = 0$  has been obtained by Honerkamp et. al. We obtain similar results when including  $t'' = -0.1t$ . Depending upon the doping

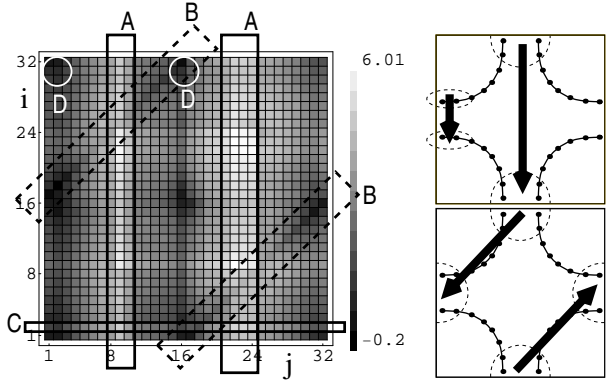


FIG. 2: The renormalized instantaneous interaction  $V_{\Lambda=0.2t}(\mathbf{k}_F(i), \mathbf{k}_F(j), \mathbf{k}_F(l))$  plotted as a function of  $i$  and  $j$  for a fixed  $l = 2$ . The solid vertical boxes (A) enclose couplings which promote commensurate and incommensurate magnetic ordering around  $(\pi, \pi)$ . Examples of these scattering processes are shown on the right with each dashed arc enclosing a segment of the Fermi surface involved in the scattering processes. The dashed diagonal boxes (B) enclose couplings which promote d-wave superconductivity. The solid horizontal box (C) encloses couplings which lead to the Pomeranchuk instability. The circles (D) enclose couplings which lead to 4 lattice constant charge-density-wave order.

level, several groups have found that the renormalization flow enhances instantaneous couplings which favor either SDW formation or d-wave superconductivity as the most prominent ordering tendency[1–3]. These can be seen in Fig. (2) where  $V_{\Lambda=0.2t}(\mathbf{k}_F(i), \mathbf{k}_F(j), \mathbf{k}_F(l))$  is plotted as a function of  $i$  and  $j$  for a fixed  $l = 2$ . The couplings which favor SDW ordering have a positive amplitude and constant momentum transfer  $\mathbf{k}_F(j) - \mathbf{k}_F(l)$ [1]. They show up as the vertical bands in boxes (A) of Fig. (2). The values  $\mathbf{k}_F(j) - \mathbf{k}_F(l)$  of these scattering processes are around  $(\pi, \pi)$ . In particular they include  $(\pi \pm 2\pi/8a, \pi)$ , indicating “incommensurate” SDW ordering. The couplings which favor d-wave superconductivity are the diagonal lines enclosed in boxes (B) of Fig. (2). These scatterings occur in the cooper channel where  $\mathbf{k}_F(i) + \mathbf{k}_F(j) = 0$ , and have an alternating sign structure indicative of d-wave symmetry. The fact that the couplings favoring superconducting pairing overlap with the couplings favoring SDW ordering signifies that physically, these ordering tendencies are linked. *Since the phonon-mediated retarded couplings do not influence the flow of the instantaneous interactions, the d-wave superconducting pairing seen above can not be due to the electron-phonon interaction.* In the present calculation, due to the choice of chemical potential and  $U$ , the spin-density waves are always the leading ordering tendency.

In addition to these two types of interactions, there also exist weaker scattering processes which favor other types of ordering. Couplings which lead to these ordering tendencies are also indicated in Fig. (2). The first is

the Pomeranchuk instability, which leads to a  $x^2 - y^2$ -symmetry deformation of the Fermi surface[3]. The second leads to a charge-density wave order with ordering wavevector equal to the vectors connecting the parallel segments of the Fermi surface near the Brillouin zone face. These wavevectors correspond to a spatial period near four lattice constants. It is worth noting that the  $t'$  and  $t''$  terms in the band structure are responsible for the almost nested Fermi surface near the Brillouin zone face. They enhance the charge ordering tendency.

Now we investigate the flow of the retarded couplings. By experimenting with the symmetries of the initial scattering amplitude, we find three independent sets of retarded interactions that are most strongly enhanced by the RG (see Fig. (3)). In all three sets the scattering amplitude shows a  $x^2 - y^2$  symmetry in momentum space. This type of sign structure can arise from phonon mediation so long as  $g(\mathbf{k}, \mathbf{k} + \mathbf{Q})$  in Eq. (4) transforms as  $\cos(k_x) - \cos(k_y)$ . For the interactions in Figs. (3a), (3b), and (3c),  $\mathbf{Q} \sim (\pm\pi, \pm\pi)$ ,  $\mathbf{Q} \sim (\pm 2\pi/4a, \pm 2\pi/4a)$ , and  $\mathbf{Q} \sim (\pm 2\pi/4a, 0), (0, \pm 2\pi/4a)$ , respectively. For example, it can arise from coupling to the half breathing or the  $B_{1g}$  [11] phonons. Note that the electron-phonon interaction with the  $B_{1g}$  buckling mode has no amplitude for momentum transfer  $(\pi, \pi)$ [17] and so will not have appreciable contribution to retarded interaction (3a). Consistent with previous results[12–15], the same analysis indicates that an s-symmetry electron-phonon coupling will be suppressed under RG. Another common feature among the three sets is that the involved initial and final momenta are all within the antinodal region.

We find that the most important contribution to the RG flow of the retarded interaction comes from the “bubble” diagram in the lower left of Fig. (1)(a), when one of vertices is an instantaneous interaction from the boxes (A) of Fig. (2) and the other is a retarded interaction. The  $x^2 - y^2$  sign structure discussed above is essential for the growth of the scattering amplitude: the positive(negative) retarded coupling combines with the instantaneous interactions to drive the negative(positive) retarded interaction to strong coupling. Since the boxes (A) enclose interactions that favor SDW ordering near  $(\pi, \pi)$ , we conclude that *commensurate and incommensurate magnetic fluctuations are responsible for driving the relevant retarded interactions to strong coupling*.

The key features of each set of retarded interactions in Fig. (3) appear as horizontal bands. In a horizontal band the momentum transfer  $\mathbf{k}_F(i) - \mathbf{k}_F(l)$  is fixed, suggesting that these couplings promote some type of density wave order. However, the  $x^2 - y^2$  sign structure makes the corresponding density wave order an unconventional one. The density wave order parameter driven by the retarded interactions in Fig. (3) has the form

$$O = \sum_{\mathbf{k}, \sigma} f(\mathbf{k}) \langle c_{\mathbf{k} + \mathbf{Q}, \sigma}^\dagger c_{\mathbf{k}, \sigma} \rangle, \quad (5)$$

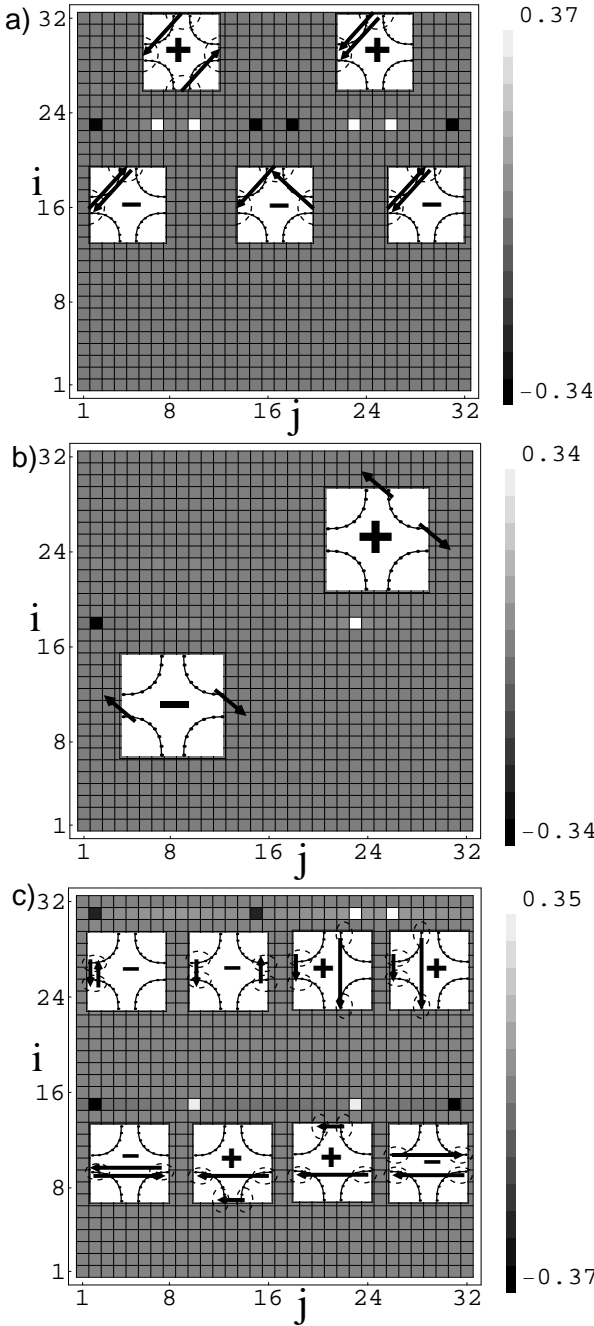


FIG. 3: The three enhanced sets of retarded interactions, with their major types of scattering processes plotted as in Fig. (2).  $\mathbf{k}_F(l)$  is fixed at  $l = 2$ . Each set of retarded interactions has both positive and negative couplings. The sign structure is indicative of a  $x^2 - y^2$  symmetry in momentum space.

where  $f(\mathbf{k})$  transforms like  $\cos(k_x) - \cos(k_y)$  under rotation. These are examples of generalized d-wave density orders, which in general can have bond averages  $\langle c_i^\dagger c_j \rangle$  with any complex phase, leading to both bond current and charge density orders[18]. We have verified via mean field calculations (details in a later publication) that all

three interactions can promote real space modulations in both charge density and current. In particular, the interaction of Fig.(3c) can lead to periodic charge density modulations with period  $\sim 4a$ . Note that the chemical potential  $\mu$  can change the nesting wavevector and hence the period of modulations. Thus we find that in the cuprates *the most important effect of the electron-phonon interaction is to promote density wave order*. Interestingly, for any order described by Eq. (5), the nodal quasiparticles will be unaffected. In particular the density wave order in Fig.(3c) is consistent with the STM experiment of Hanaguri *et al* and the ARPES experiment by Shen *et al*. In addition, the fact that all the enhanced retarded interactions in Fig. (3) involve scattering processes with initial and final momentum states in the antinodal region is also consistent with the isotope-dependent ARPES study of Ref.[7].

Acknowledgement: We are in debt to J.C. Davis, K.P. McElroy, G.-H. Gweon, A. Lanzara, K. Shen, Z.-X. Shen, D. Scalapino, W. Hanke, and W. Metzner for many discussions. DHL is supported by DOE grant DE-AC03-76SF00098. HCF was partially supported by a predoc-toral fellowship from the Advanced Light Source.

---

[1] C. Honerkamp, M. Salmhofer, N. Furukawa, and T. M. Rice, Phys. Rev. B **63**, 135109 (2001).  
[2] D. Zanchi and H. J. Schulz, Europhys. Lett. **44**, 235(1997); Phys. Rev. B **61**, 13609 (2000).  
[3] C. J. Halboth and W. Metzner, Phys. Rev. Lett. **85**, 5162 (2000).  
[4] X. J. Zhou et al., Phys. Rev. Lett **92**, 187001 (2004).  
[5] T. Hanaguri et al., Nature **430**, 1001 (2004).  
[6] K. M. Shen et al., Science **307**, 901 (2005).  
[7] G.-H. Gweon et al., Nature **430**, 187 (2004).  
[8] G. T. Zimanyi, S. A. Kivelson, and A. Luther, Phys. Rev. Lett. **60**, 2089 (1988).  
[9] A. Seidel, H.-H. Lin, and D.-H. Lee, Phys. Rev. B **71**, 220501 (2005).  
[10] H. C. Fu, A. Seidel, H.-H. Lin, and D.-H. Lee (2006), to be published.  
[11] T. P. Devereaux, T. Cuk, Z.-X. Shen, and N. Nagaosa, Phys. Rev. Lett. **93**, 117004 (2004).  
[12] J. H. Kim, K. Levin, R. Wentzcovich, and A. Auerbach, Phys. Rev. B **44**, 5148 (1991).  
[13] M. Grilli and C. Castellani, Phys. Rev. B **50**, 16880 (1994).  
[14] R. Zeyher and M. L. Kulic, Phys. Rev. B **53**, 2850 (1996).  
[15] Z. B. Huang, W. Hanke, E. Arrigoni, and D. J. Scalapino, Phys. Rev. B **68**, 220507 (2003).  
[16] T. Cuk, D. H. Lu, X. J. Zhou, Z. X. Shen, T. P. Devereaux, and N. Nagaosa, Physica Stat. Sol. B-Basic Research **242**, 11 (2005).  
[17] O. Jepsen, O. K. Andersen, I. Dasgupta, and S. Savrasov, J. Phys. Chem. Solids **59**, 1718 (1998).  
[18] S. Chakravarty, R. B. Laughlin, D. K. Morr, and C. Nayak, Phys. Rev. B **63**, 094503 (2001).